Anelastic deformation of a Pd 40 Cu 30 Ni 10 P 20 bulk metallic glass during nanoindentation

A. Concustell, J. Sort, A. L. Greer, and M. D. Baró
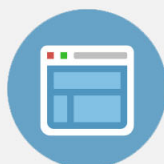
Anelastic deformation of a $Pd_{40}Cu_{30}Ni_{10}P_{20}$ bulk metallic glass during nanoindentation

A. Concustell[a)]
Departament de Física, Edifici Cc, Universitat Autònoma de Barcelona,
08193 Bellaterra, Barcelona, Spain

J. Sort
Institució Catalana de Recerca i Estudis Avançats and Departament de Física, Universitat Autònoma
Barcelona, 08193 Bellaterra, Barcelona, Spain

A. L. Greer
Department of Materials Science and Metallurgy, University of Cambridge, Pembroke Street,
Cambridge CB2 3QZ, United Kingdom

M. D. Baró
Departament de Física, Edifici Cc, Universitat Autònoma de Barcelona,
08193 Bellaterra, Barcelona, Spain

Time-dependent deformation processes during nanoindentation have been investigated on a $Pd_{40}Cu_{30}Ni_{10}P_{20}$ bulk metallic glass. Deformation under constant load has been studied as a function of prior loading rate and temperature. The constant-load displacement of the indenter into the sample shows classic relaxation kinetics and reveals the importance of anelasticity for the mechanical behavior of metallic glasses at the nanoscale. © *2006 American Institute of Physics.*
[DOI: 10.1063/1.2198517]

Some bulk metallic glasses (BMGs) and amorphous ribbons exhibit outstanding mechanical properties,[1–5] and good corrosion and wear resistance.[6] This makes them attractive as structural materials.[7] However, plasticity before fracture of BMGs is very limited in uniaxial tensile tests, although it is extended under compression tests.[8–10] This has been explained as a consequence of their plastic deformation being governed by strain localization in shear bands.[11] Recently, several authors have studied the mechanisms of plastic deformation in BMGs by means of nanoindentation.[12–17] In nanoindentation of BMGs, plastic deformation is manifested as pop-in events on the load-displacement curves during loading.[12] These serrations, which are more pronounced for low loading rates, have been related to the formation and propagation of shear bands.[14–17]

Although plastic deformation during nanoindentation has been studied to some extent in BMGs, time-dependent deformation effects have generally been overlooked. Apart from its fundamental interest, the creep of submicrometer contacts is also of clear practical significance. Such contacts are inevitable, in micromechanical systems, and their excessive creep may lead to undesirable changes in device performance. Furthermore, the values of hardness and the reduced elastic modulus, derived from the method of Oliver and Pharr,[18] can be in error because of indentation-creep effects.[19] Time-dependent deformation during nanoindentation tests can occur by the diffusion and motion of atoms in the indentation stress field, the extent of which depends on temperature.

The current work focuses on the time dependence of deformation during nanoindentation tests on a BMG. The deformation of the material under constant load has been studied as a function of temperature and loading rate.

A master alloy with composition $Pd_{40}Cu_{30}Ni_{10}P_{20}$ (at. %) was prepared by arc melting a mixture of the pure elements under argon. A cylinder of 5 mm diameter and 50 mm length was cast in a Cu mold under argon. The surface for nanoindentation was obtained by cutting the cast rod perpendicular to its axis and mechanically polishing to mirror finish. Nanoindentation was performed in ambient air using a *Micro Materials NanoTest 600* with a pyramidal Berkovich indenter. The load-time sequence (Fig. 1) consists of two loading segments followed by two constant-load segments of 150 s duration (hold 1 and hold 3 in the figure) and two unloading segments at 1 mN s^{-1}. Different loading rates (0.2, 0.5, 1.0, and 2.0 mN s^{-1}) were used, keeping the same rate in both loading segments of a given sequence. A low-load segment of 60 s (hold 2) was also introduced between the two loading segments to measure the thermal drift. The second load-unload cycle was added to seek evidence for possible plastic deformation during the first load-unload cycle. A hot stage was used to perform nanoindentation experiments, in air, at different temperatures (298, 311, 323, and 336 K). Ten nanoindentation tests were carried out under each set of con-
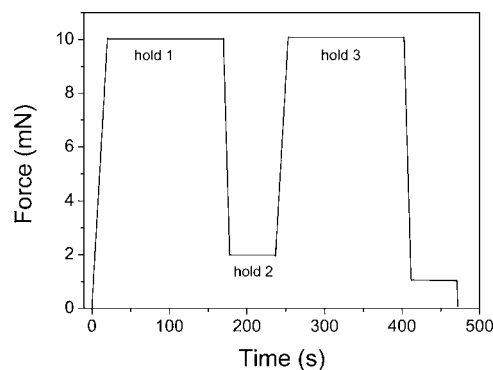

FIG. 1. Schematic representation of the load-unload sequence used for the nanoindentation tests.

a)Electronic mail: amadeu.concustell@uab.es

TABLE I. Dependence of the hardness H and the reduced elastic modulus E_r on the indentation loading rate dF/dt at room temperature.

	dF/dt (mN s^{-1})			
	2.0	1.0	0.5	0.2
H (GPa)	4.7±0.2	4.6±0.2	4.6±0.2	4.5±0.2
E_r (GPa)	114±2	110±3	110±3	109±3

ditions. The hardness and the reduced elastic modulus were derived using the method of Oliver and Pharr.[18]

From the maximum penetration depths at the end of hold 1 and hold 2 it is possible to evaluate the overall plastic deformation occurring during the first load-unload cycle. For sharp indenters with fully elastic loading and unloading, the penetration depth h is linearly proportional to $F^{1/2}$, where F is the applied load.[20,21] Thus, extrapolating to $F=0$, one can obtain the overall plastic deformation, which was found to be around 150 nm for all the investigated loading rates.

Figure 2(a) shows the time evolution of the indenter displacement into the sample during the first constant-load segment, for different loading rates at 298 K. Whatever the indentation rate, the indenter continues to penetrate into the material after the maximum load has been reached. For higher loading rates the penetration is more pronounced, but the overall maximum indentation depth after the first constant-load segment is similar in all cases. This is contrary to what was reported in Ref. 16, where the authors used an exceedingly short (i.e., 2 s) holding segment. As a consequence, the hardness and the reduced elastic modulus are independent of the loading rate, as shown in Table I. Remarkably, for a given loading rate, the overall penetration depth obtained after the second loading+hold 3 is the same as that after the first loading+hold 1.

Nanoindentation was also performed at different temperatures. Figure 2(b) shows the h versus time dependences for the first constant-load segment, for experiments at a loading rate of 2 mN s^{-1}. The penetration is greater at lower temperatures. But at a given temperature, the final indentation depth after the loading+constant-load segments is approximately independent of the loading rate.

The displacements of the indenter into the sample during hold 1 and hold 3 show classic relaxation kinetics, described in the simplest case by
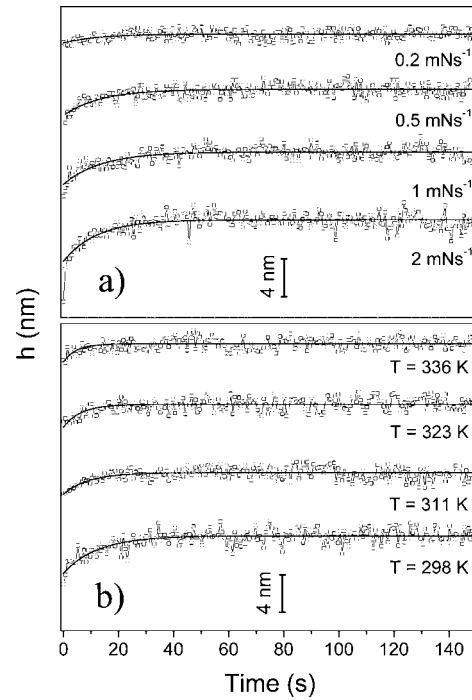

FIG. 2. Time dependence of the indenter displacement into the sample, h, during the first constant-load segment: (a) for different loading rates, all measured at 298 K, and (b) for different temperatures, all at a loading rate of 2 mN s^{-1}. The continuous lines are fits to the data using Eq. (1).

$$h(t) = h_0 \left[1 - \exp\left(-\frac{t}{\tau}\right) \right], \qquad (1)$$

where t is the time, h_0 is the ultimate additional penetration that takes place during the constant-load segment, and τ is the characteristic relaxation time. Fitting of the data in Figs. 2(a) and 2(b) to Eq. (1) gives the τ values quoted in Table II. The experimental values of the penetration depth during the constant-load segments, $h_{0,\text{expt}}$, are also shown in Table II. For the experiments performed at the same temperature, τ is similar for all constant-load segments, independent of the loading rate. However, $h_{0,\text{expt}}$ increases with loading rate and is larger for hold 1 than for hold 3 (Table II). Moreover, comparison of the curves in Fig. 2(b) shows that time-dependent deformation occurs faster at higher temperatures.

The similarity of the relaxation times at a given temperature, independent of the loading rate and the constant-load segment, suggests that the mechanism of deformation is the same for all constant-load segments. The uniformity of over-

TABLE II. Dependence of relaxation time τ and the penetration depth during the holding segments, $h_{0,\text{expt}}$, on the temperature and the loading rate. Some values are missing because they are too small.

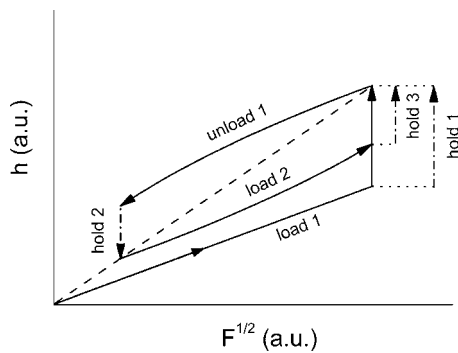| Fitted parameters	dF/dt (mN s^{-1})	Temperature (K)							
		298		311		323		336	
		Hold 1	Hold 3	Hold 1	Hold 3	Hold 1	Hold 3	Hold 1	Hold 3
τ (s)	2.0	12.5	13.6	9.3	9.0	6.5	6.1	4.6	4.6
	1.0	12.7	13.1	9.5	9.1	6.2	6.3	⋯	⋯
	0.5	13.2	11.4	9.4	9.3	6.2	6.3	⋯	⋯
	0.2	12.5	12.7	⋯	⋯	⋯	⋯	⋯	⋯
$h_{0,\text{expt}}$ (nm)	2.0	7.5	5.3	4.8	2.8	2.6	1.3	2.2	1.4
	1.0	6.1	3.3	3.2	2.3	2.2	1.6	⋯	⋯
	0.5	5.0	3.8	2.4	1.7	1.5	1.4	⋯	⋯
	0.2	3.4	1.6	⋯	⋯	⋯	⋯	⋯	⋯

FIG. 3. Schematic representation of the overall anelastic material behavior during the nanoindentation experiments. The discontinuous line indicates the equilibrium elastic response of the material.

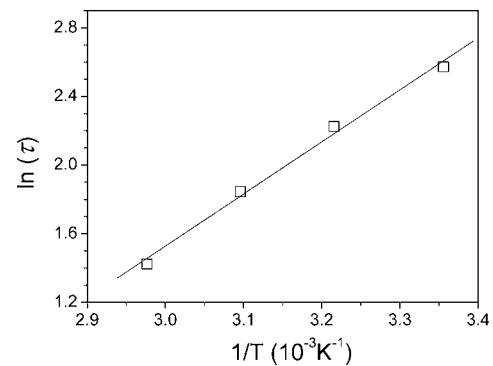
FIG. 4. Logarithm of the mean of the observed relaxation times τ at each temperature as a function of $1/T$. The straight line is a fit to the data.

all maximum depths obtained after the first and second loading and constant-load segments indicates that the material first behaves anelastically and then exhibits no time-dependent plastic deformation during the second nanoindentation cycle. Plastic deformation during hold 1 must also be rather small, as there are no pop-in events in the h versus time curves of Fig. 2. Thus, plastic deformation occurs mainly during the first loading segment. The penetration during the constant-load segments ($h_{0,\text{expt}}$) is larger for faster prior loading, since the material has had less time, during loading, for anelastic strains to reach the stable elastic state.

The effects of anelasticity on the elastic contribution to the overall material deformation are schematically represented in Fig. 3. This figure explains why the penetration during hold 1 is larger than during hold 3. During hold 2 the material shows anelasticity and it is completely relaxed. Hence, when the indenter again applies a constant loading rate during the second loading segment, the material deforms from a different elastic state, with higher elastic modulus, than in the first loading segment. As a result, $h_{0,\text{expt}}$ for hold 3 is always lower than for hold 1 (Fig. 3).

Since anelastic flow is thermally activated, the relaxation time decreases with increasing temperature, each value of the distributed relaxation time taking the form[22–24]

$$\tau = \tau_0 \exp\left(\frac{Q}{kT}\right), \tag{2}$$

where Q is the activation energy of the process, τ_0 is a pre-exponential factor, k is Boltzmann's constant, and T is the absolute temperature. In Fig. 4, the logarithm of the relaxation time at each temperature is plotted as a function of $1/T$. From Eq. (2), an effective activation energy can be evaluated to be 0.26 eV atom^{-1}, smaller than, for example, the energy of a vacancy formation in a Pd crystalline alloy.[25] Anelasticity in metallic glasses is a process distributed over a range of activation energies.[23] Ocelík *et al.* have studied the influence of the loading time on the calculated spectra of activation energies for the anelastic processes in an amorphous ribbon.[22] In particular, a fully developed spectrum was observed only for long enough loading times (>100 s) and high enough temperatures (e.g., 618 K). It was concluded that anelastic processes with longer relaxation times were not activated at faster loading rates. The low temperatures and high loading rates used in the present experiments favor anelastic deformation processes with shorter relaxation times, the ones with longer τ (i.e., with larger Q) failing to be activated and therefore not taking part in the recovery.[22] Moreover, at high temperatures, the penetration during the constant-load segments decreases because the characteristic relaxation time is so short that partial anelastic recovery can occur during the loading.

The microscopic mechanisms of short-time and low-temperature anelastic relaxation are similar to those for reversible annealing-induced structural relaxation.[23] The low activation energy and short relaxation time found in our case suggest that local atomic shear motions, changing only the local shear stress but breaking no atomic bonds, are responsible for the observed anelasticity.

[1] A. Gebert, U. K. Mudali, J. Eckert, and L. Schultz, Mater. Res. Soc. Symp. Proc. **806**, 369 (2004).
[2] A. Concustell, M. Zielinska, Á. Révész, L. K. Varga, S. Suriñach, and M. D. Baró, Intermetallics **12**, 1063 (2004).
[3] H. A. Bruck, T. Christman, A. J. Rosakis, and W. L. Johnson, Scr. Metall. Mater. **30**, 429 (1994).
[4] A. Leonhard, L.-Q. Xing, M. Heilmaier, A. Gebert, J. Eckert, and L. Schultz, Nanostruct. Mater. **10**, 805 (1998).
[5] M. Ohtsuki, R. Tamura, S. Takeuchi, S. Yoda, and T. Ohmura, Appl. Phys. Lett. **84**, 4911 (2004).
[6] S. J. Pang, T. Zhang, K. Asami, and A. Inoue, Acta Mater. **50**, 489 (2002).
[7] A. I. Salimon, M. F. Ashby, Y. Bréchet, and A. L. Greer, Mater. Sci. Eng., A **375–377**, 385 (2004).
[8] L. A. Davis and S. Kavesh, J. Mater. Sci. **10**, 453 (1975).
[9] T. Mukai, T. G. Nieh, Y. Kawamura, A. Inoue, and K. Higashi, Scr. Mater. **46**, 43 (2002).
[10] G. Subhash, R. J. Dowding, and L. J. Kecskes, Mater. Sci. Eng., A **334**, 33 (2003).
[11] F. Spaepen, Acta Metall. **25**, 407 (1977).
[12] Y. I. Golovin, V. I. Ivolgin, V. A. Khonik, K. Kitagawa, and A. I. Tyurin, Scr. Mater. **45**, 947 (2001).
[13] C. A. Schuh and T. G. Nieh, Acta Mater. **51**, 87 (2003).
[14] C. A. Schuh, A. C. Lund, and T. G. Nieh, Acta Mater. **52**, 5879 (2004).
[15] A. L. Greer, A. Castellero, S. V. Madge, I. T. Walker, and J. R. Wilde, Mater. Sci. Eng., A **375–377**, 1182 (2004).
[16] A. Concustell, J. Sort, G. Alcalá, S. Mato, A. Gebert, J. Eckert, and M. D. Baró, J. Mater. Res. **20**, 2719 (2005).
[17] H. Bei, Z. P. Lu, and E. P. George, Phys. Rev. Lett. **93**, 125504 (2004).
[18] W. C. Oliver and G. M. Pharr, J. Mater. Res. **7**, 1564 (1992).
[19] G. Feng and A. H. W. Ngan, J. Mater. Res. **17**, 660 (2002).
[20] Y.-T. Cheng and C.-M. Cheng, Int. J. Solids Struct. **36**, 1231 (1999).
[21] K. Zeng and C. H. Chiu, Acta Mater. **49**, 3539 (2001).
[22] V. Ocelík, K. Csach, A. Kasardová, and V. Z. Bengus, Mater. Sci. Eng., A **226–228**, 851 (1997).
[23] A. Kursumovic and B. Cantor, Scr. Mater. **34**, 1655 (1996).
[24] B. S. Berry, *Metallic Glass* (American Society for Metals, Metals Park, OH, 1976).
[25] T. R. Mattsson and A. E. Mattsson, Phys. Rev. B **66**, 214110 (2002).